Phys. Status Solidi B **253**, No. 4, 683–689 (2016) / **DOI** 10.1002/pssb.201552576

physica status solidi b
www.pss-b.com
basic solid state physics

$LiTaO_3$ phonon dispersion and ferroelectric transition calculated from first principles

Michael Friedrich*, **Arno Schindlmayr, W. G. Schmidt, and Simone Sanna**

Department Physik, Universität Paderborn, 33095 Paderborn, Germany

Received 7 September 2015, revised 28 October 2015, accepted 9 November 2015
Published online 8 December 2015

Keywords density functional perturbation theory, ferroelectrics, phase transitions, specific heat, vibrational properties

* Corresponding author: e-mail Michael.Friedrich@uni-paderborn.de, Phone: +49 5251 602328, Fax: +49 5251 603435

The phonon dispersions of the ferro- and paraelectric phase of $LiTaO_3$ are calculated within density-functional perturbation theory. The longitudinal optical phonon modes are theoretically derived and compared with available experimental data. Our results confirm the recent phonon assignment proposed by Margueron et al. [J. Appl. Phys. **111**, 104105 (2012)] on the basis of spectroscopical studies. A comparison with the phonon band structure of the related material $LiNbO_3$ shows minor differences that can be traced to the atomic-mass difference between Ta and Nb. The presence of phonons with imaginary frequencies for the paraelectric phase suggests that it does not correspond to a minimum energy structure, and is compatible with an order-disorder type phase transition.

1 Introduction Lithium tantalate ($LiTaO_3$, LT) and lithium niobate ($LiNbO_3$, LN) are related ferroelectric materials that crystallize within the $R3c$ space group below the Curie temperature and within the space group $R\bar{3}c$ above it [1]. Due to their unique combination of structural, electronic, and optical properties, both materials are widely employed for acousto-optic and electro-optic devices, such as frequency converter and modulators for optical fiber communications or for holographic data storage [2, 3]. Despite their widespread use, many fundamental characteristics of the two materials are still not completely understood. This concerns, in particular, the vibrational properties and the ferroelectric–paraelectric structural phase transition.

The knowledge of the phonon modes and frequencies in $LiNbO_3$ remained incomplete until recent experimental [4] and theoretical [5] investigations provided the first unambiguous assignment of the observed phonon frequencies at the Brillouin-zone center. Later, the full phonon dispersion was predicted theoretically [6, 7]. However, corresponding measurements away from the zone center have not yet been performed. The knowledge of the $LiTaO_3$ vibrational properties is even more fragmentary. While theory and experiment seem to agree concerning the assignment of the transversal modes at the Γ point [4, 5], only in a very recent theoretical work Toyoura et al. [6] have investigated the phonon modes at different points of the Brillouin zone.

The ferroelectric–paraelectric structural phase transition in $LiNbO_3$ occurs at 1480 K and has been under investigation for more than five decades. Different studies interpreted it either as a displacive [8–10] or order–disorder type [11–13] transition. A combined displacive and order–disorder type scenario was also proposed [14] and has found theoretical support [15–17]. Equally contradictory reports are found for $LiTaO_3$, which undergoes a ferroelectric-paraelectric structural phase transition at 940 K. While some investigations indicate a behavior compatible with a displacive transition, [18] other studies predict an order–disorder character [19]. In particular, a recent theoretical work suggested that the phase transition is not of conventional displacive type but of order–disorder type with strong correlation between cation displacements [6].

In order to improve our understanding of the vibrational properties of the two materials, we calculate in this work the complete $LiTaO_3$ phonon dispersion over the first Brillouin zone from *first principles*. The outcome of our calculations is compared with the $LiNbO_3$ phonon dispersion obtained with the same approach [7], which is based on density-functional perturbation theory. The calculated phonon frequencies are then employed to estimate the Curie temperatures of $LiTaO_3$ and $LiNbO_3$. Our calculations indicate that the free energies of the para- and ferroelectric phase nearly coincide for temperatures above 1150 K (LN) and 770 K

Table 1 Calculated $LiTaO_3$ lattice parameters. Experimental data from Abrahams et al. [36] at 297 K for the ferroelectric phase and at 940 K for the paraelectric phase are reported for comparison. Ω^{PE}_{Expt} denotes calculations that were performed at the unit-cell volume measured at 940 K to simulate thermal expansion.

ferroelectric	a/Å	c/Å	u	v	w	z
Ω^{FE}_{Theory}	5.129	13.678	0.0094	0.0421	0.0125	0.0327
Ω^{PE}_{Expt}	5.211	13.810	0.0082	0.0525	0.0130	0.0328
experiment	5.154	13.783	0.0103	0.0398	0.0146	0.0290
paraelectric	a/Å	c/Å	x			
Ω^{PE}_{Theory}	5.169	13.568	0.0501			
Ω^{PE}_{Expt}	5.234	13.692	0.0570			
experiment	5.220	13.763	0.0531			

(LT), which can thus be regarded as lower bounds for the transition temperature. Additionally, for $LiTaO_3$ we present the first theoretical modeling of the longitudinal optical (LO) phonon frequencies at the Γ point based on the density-functional perturbation theory. Our calculations are compared with experimental data [4, 5] and calculations based on the finite-differences method, and confirm the recent assignment proposed in Ref. [4].

2 Computational method We perform our calculations using density-functional theory [20, 21] (DFT) as well as density-functional perturbation theory [22–25] (DFPT) as implemented in the ABINIT package [26–28]. The electron exchange and correlation interaction is treated with the PBEsol functional parameterized by Perdew et al. [29], which is optimized for solids. In the optimized norm-conserving Vanderbilt pseudopotentials [30], the 1s and 2s orbitals of lithium, the 2s and 2p orbitals of oxygen, as well as the 5p, 5d, and 6s orbitals of tantalum are treated as valence states. Convergence of the total electronic energy within 1×10^{-5} Hartree is achieved with a kinetic cut-off energy of 38 Hartree for the plane-wave basis and a Monkhorst–Pack [31] mesh of 4×4×4 **k** points. After structure optimization the forces on the atoms are lower than 5×10^{-7} Hartree/Bohr. A 4×4×4 **q**-point mesh is required for the calculation of the phonon band structure in order to obtain vibrational frequencies converged within 1 cm^{-1}.

For vanishing pressure the ground state of an insulating solid at temperature T is characterized by the minimum of the free energy $F = F^e + F^{vib}$, where $F^e = E^e - TS^e$ is the electronic free energy and F^{vib} the vibrational free energy. The electronic entropy S^e plays a minor role in the investigated materials due to the large electronic band gaps of LN [33] and LT [34] and is neglected in this work. The ground-state energy E^e is approximated by the zero-temperature DFT value. The vibrational free energy per unit cell is calculated within the harmonic approximation

$$F^{vib} = \frac{\Omega}{8\pi^3}\sum_{j=1}^{3n}\int\left[\frac{1}{2}\hbar\omega_j(\mathbf{q}) + k_B T\ln\left(1-e^{-\frac{\hbar\omega_j(\mathbf{q})}{k_B T}}\right)\right]d^3q, \quad (1)$$

where Ω is the cell volume, $\omega_j(\mathbf{q})$ the frequency of mode j, and **q** a vector of the Brillouin zone. A mesh of 14×14×14 **q** points is used for the integration, leading to a numerical error below 1 meV.

3 Results

3.1 Structural data Up to about 940 K stoichiometric $LiTaO_3$ belongs to the space group $R3c$ and is ferroelectric [35]. Above this temperature LT undergoes a structural phase transition to the paraelectric phase with space group $R\bar{3}c$. Both structures are investigated in this work. The calculated structural parameters of fully relaxed unit cells are compiled in Table 1. Although the calculations are performed with the rhombohedral primitive cell, the structural properties are given in terms of the more common hexagonal setting, where a and c denote the lattice parameters, while u, v, w, z, and x control the atomic positions within the ferro- and paraelectric unit cell, respectively (see Ref. [7] for details). The results are compared with experimental data from Abrahams et al. [36] obtained from neutron scattering at 297 and 940 K.

The lattice parameters of ferroelectric LT are in very good agreement with the experimental findings, which are reproduced with a deviation of at most 0.7%. The deviation from the experimental data of the paraelectric phase is somewhat higher, with the largest discrepancy observed for the parameter c, which is underestimated by 1.4%. The underestimation of the lattice parameters is due to the thermal expansion of the material at high temperatures (e.g., 940 K), which is not considered in DFT calculations. The lattice parameters corresponding to the calculated equilibrium volume are labeled by Ω^{PE}_{Theory}. In order to include the thermal expansion in the subsequent phonon and free-energy calculations, we also relax the structure at the experimental unit-cell volume measured at 940 K. The corresponding results are labeled by Ω^{PE}_{Expt}. As there is no experimental evidence for a volume change at the phase transition, Ω^{PE}_{Expt} represents both the volumes of the ferroelectric unit cell and of the paraelectric unit cell at the considered temperature. Within this approach, we obtain a unit cell that is slightly distorted in comparison to the data from Abrahams et al. [36]. Consequently, the internal parameters are slightly overestimated. Similar deviations were recently noticed when modeling $LiNbO_3$ [7].

Table 2 Calculated TO and LO zone-center frequencies in cm^{-1} for the ferroelectric phase (Ω^{FE}_{Theory}) compared to experimental measurements from Ref. [5].

mode	TO	expt.	LO	expt.
A_1	204	209–210	396	403
	258	256–257	258	255
	356	359–360	352	355
	581	600	842	866
E	144	143	191	190
	196	210	196	
	248	254–257	277	279
	312	315–317	334	344*
	360	383–384	444	453
	373	383–384	373	381
	456	460–465	465	476*
	579	592	838	866
	660	661–662	660	660

*Found only by Margueron et al. [4].

3.2 Phonons at the Brillouin-zone center The optical phonon frequencies calculated for ferroelectric LT at the Γ point are presented in Table 2. The transversal optical (TO) frequencies are compared to recent measurements [5]. The overall agreement with the Raman data is very good, with an underestimation of the measured values of, on average, 2%. The largest deviation of about 20 cm^{-1} occurs for the A_1 TO_4 mode. The excellent agreement with the experiment for all A_1 and E frequencies is due to the accuracy of the structural parameters and to a particular form of error cancelation [38]: it is known that phonon calculations within DFPT tend to underestimate the vibrational frequencies, while the underestimation of the unit-cell volume gives rise to increased frequencies. Unexpectedly, the deviations of the internal parameters do not lead to scattering around the experimental values. The Raman inactive A_2 modes can, in principle, be experimentally determined, e.g., by neutron scattering. Unfortunately, no such data is presently available. We predict the A_2 modes to be at 180, 283, 379, 448, and 908 cm^{-1}.

In addition to the transversal modes, we present the first theoretical estimate based on the DFPT of the longitudinal optical (LO) phonons at Γ, which are also found in very good agreement with the experimental data (Table 2, right column). Thereby, we identify two E modes, which have not been reported in our previous work [5] but are experimentally confirmed by Margueron et al. [4]. The order of frequencies in Table 2 is chosen such as to ease the assignment of related LO and TO modes. The correspondence between the TO and LO modes is established by means of the overlap $\sum_{\alpha,\kappa} M_\kappa U^{LO}_{j\alpha\kappa} U^{TO}_{j'\alpha\kappa}$, where j is the index of the phonon mode, $U_{j\alpha\kappa}$ the element of the phonon eigenvector $\mathbf{U_j}$ corresponding to the Cartesian direction α and κ-th atom, and M_κ is the mass of atom κ [39].

Concerning the A_1 modes, the overlaps between the transversal and longitudinal phonon eigenvectors are 0.9994 and 0.8118 for the second and third mode, respectively, indicating that these modes are not, or only slightly, influenced by the macroscopic electric field. In contrast to the expectation that the additional forces of the macroscopic electric field always give rise to higher phonon frequencies, the third LO mode is lower than the third TO mode, which we relate to minor deviations of the respective eigenvectors. In case of the E modes we clearly observe no splitting of TO modes number 2, 6, and 9, as the overlap between them amounts to 100%, which is basically in agreement with Refs. [4, 5]. Their low Raman intensities are responsible for the fact that some modes have not been observed previously. The fourth LO E mode could only be identified in the infrared data of Margueron et al. [4].

Table 3 Calculated zone-center frequencies of the paraelectric phase with the theoretical lattice constants (Ω^{PE}_{Theory}).

mode	frequencies (cm^{-1})				
A_{1g}	377				
A_{1u}	232	384			
A_{2g}	95i	426	910		
A_{2u}	163i	162	522		
E_g	178	413	481	632	
E_u	118	201	325	419	560

As the paraelectric phase is only stable at very high temperatures, a measurement of the vibrational properties is very challenging and has not been yet performed. Nonetheless, in Table 3 we report the TO frequencies calculated for the paraelectric phase at the theoretically determined volume. The presence of imaginary frequencies reveals that the paraelectric phase is not stable at 0 K. We observe two imaginary modes, which correspond to saddle points of the potential energy surface. This is illustrated in Fig. 1. Similar to lithium niobate, the displacement pattern of the lowest A_{2u} mode is almost identical to the paraelectric–ferroelectric phase tran-

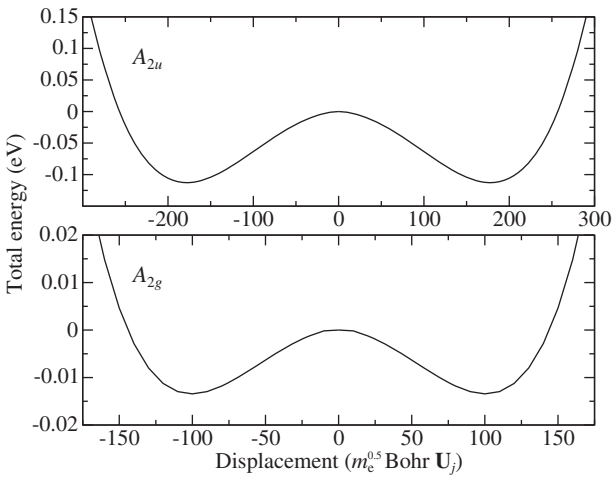

Figure 1 Variation of the DFT total electronic energy with respect to the atomic displacement according to the eigenvector of the unstable A_{2u} and A_{2g} phonon modes.

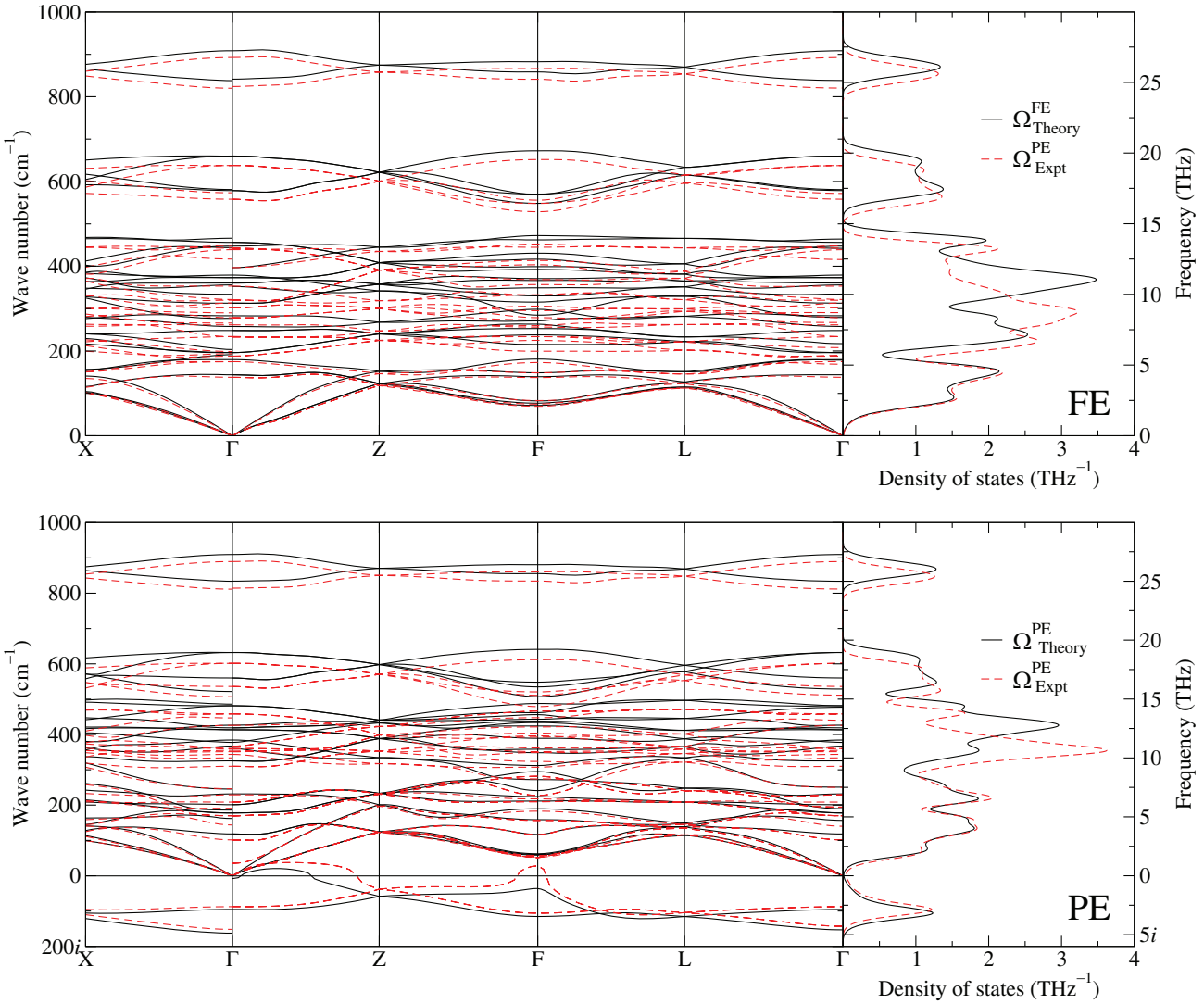

Figure 2 Phonon dispersion and density of states of ferroelectric (top) and paraelectric (bottom) $LiTaO_3$.

sition with the parameter values 0.0101, 0.0441, 0.0139, and 0.0319 for u, v, w, and z, respectively, corresponding to the minimum of the total energy at a displacement of the atoms of $175\sqrt{m_e}$ Bohr times the phonon eigenvector of the lowest A_{2u} mode. It can also be observed in Fig. 1 that the energy difference between the unstable saddle-point position and the energetic minimum is almost ten times larger for the A_{2u} mode than for the A_{2g} mode, which again shows that the mode A_{2u} drives the phase transition.

3.3 Phonon dispersion The phonon dispersion relation for the ferroelectric and paraelectric phase of $LiTaO_3$ is shown in Fig. 2. In order to facilitate the comparison with the $LiNbO_3$ phonon dispersion presented in previous works [7, 40], we choose the path X–Γ–Z–F–L–Γ in the Brillouin zone.

The calculated phonon dispersion of $LiTaO_3$ strongly resembles that of $LiNbO_3$. This is not surprising due to the very similar crystal structures of both materials. The main differences can be observed in the density of states of the ferroelectric phase around 200 cm^{-1}, which is lower than for lithium niobate. This is due to the large mass mismatch between the heavy Ta and the light Li and O atoms, which largely decouples some atomic displacements. This can be illustrated by comparing the atom-resolved phonon densities of states of both materials (see Fig. 3).

In the paraelectric phase, no unstable E modes are observed at Γ and F, unlike in the case of LN. Even the A_{2g} mode becomes partially stable due to the macroscopic electric field (longitudinal optical phonon modes). This might be due to the relaxation and the different lattice parameters for both materials. To demonstrate the impact of thermal expansion, the calculated dispersion corresponding to the larger volume Ω^{PE}_{Expt} is also shown in Fig. 2. As expected, these frequencies are lower due to the larger lattice constants, but there are also slight differences due to the change of the internal parameters.

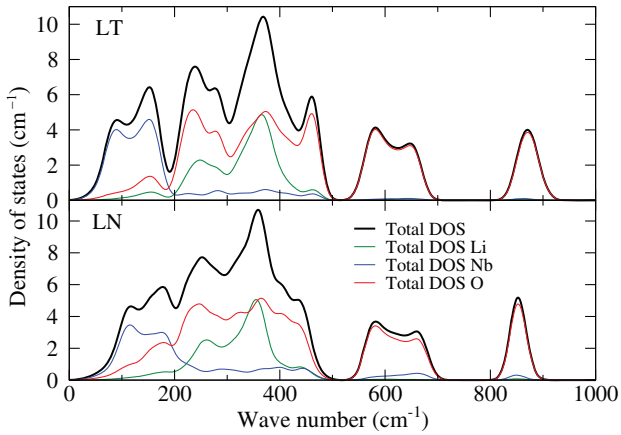

Figure 3 Comparison of the atom-resolved phonon densities of states of LT and LN.

In order to make sure that the presence of imaginary modes at different **k** points in the Brillouin zone is not an artifact of the DFPT method, we have also calculated the phonon frequencies at two different points of the Brillouin zone of the rhombohedral structure (Γ and L) with the finite-difference method at the experimental volume $\Omega^{\mathrm{PE}}_{\mathrm{Expt}}$. The results of the calculations are shown in Table 4. All the modes at L are doubly degenerate. The frequencies calculated with the two methods are in very good agreement and show a deviation of merely few cm^{-1}. In particular, the imaginary frequencies predicted with DFPT are also predicted by the finite-difference method. As these modes have imaginary frequencies almost everywhere in the reciprocal space, the paraelectric phase clearly does not correspond to a minimum energy structure.

The calculated phonon dispersions and phonon densities of states in Figs. 2 and 3 can be directly compared with the phononic bands recently calculated by Toyoura et al. [6] with the finite-differences method. The high-energy phonon branches disperse more strongly in Ref. [6], possibly due to the different treatment of the TO–LO splitting and the interpolation scheme used in that work to derive the phonon energies between high-symmetry points. Nonetheless, the curves calculated with the two complementary methods are in good overall agreement. In particular, for the lower and imaginary frequencies in the paraelectric phase a close correspondence between the results is observed. These modes, involving Li displacements along the crystal *c* axis, are crucial for the ferroelectric phase transition. Their imaginary frequency values in most of the reciprocal space are compatible with an order–disorder transition type [6].

In order to check the accuracy of the calculated phonon dispersion, we employ it to calculate the specific heat capacity with the approach implemented in ABINIT [26–28]. This leads to a theoretical value of 402 J kg^{-1} K^{-1} at 298 K, which is in the range of the experimental uncertainty of the value (426 ± 36) J kg^{-1} K^{-1} determined by Glass [41] using light pulses to heat the stoichiometric probe and recording the temperature change. This lower theoretical value in comparison to $LiNbO_3$ (651 J kg^{-1} K^{-1}) [7] is explained by the much higher atomic mass of tantalum compared to niobium.

Table 4 Phonon frequencies of the paraelectric phase of $LiTaO_3$ and $LiNbO_3$ calculated with the finite-differences method at the Γ and L point of the rhombohedral Brillouin zone at $\Omega^{\mathrm{PE}}_{\mathrm{Expt}}$. The mode symmetry at Γ is indicated, frequencies are in cm^{-1}.

$LiTaO_3$		$LiNbO_3$	
Γ	L	Γ	L
151*i* (A_{2u})	97*i*	206*i* (A_{2u})	101
71*i* (A_{2g})	114	133*i* (E_u)	129
108 (E_u)	138	71*i* (A_{2g})	152
153 (A_{2u})	146	48 (A_{2u})	162
178 (E_g)	206	168 (E_g)	204
196 (E_g)	244	187 (E_u)	245
228 (A_{1u})	332	268 (A_{1u})	335
321 (E_u)	360	362 (A_{1g})	345
381 (A_{1g})	384	365 (E_u)	367
388 (A_{1u})	412	388 (E_g)	392
411 (E_g)	446	390 (E_u)	413
419 (E_u)	494	400 (A_{1u})	473
421 (A_{2g})	566	402 (A_{2g})	487
479 (E_g)	586	444 (A_{2u})	512
507 (A_{2u})	857	448 (E_g)	817
554 (E_u)		491 (E_u)	
622 (E_g)		539 (E_g)	
898 (A_{2g})		845 (A_{2g})	

3.4 Phase transition The ground state of a compound at a given temperature corresponds to the structural phase associated with the lowest free energy *F*. The point at which the difference between the free energies of two competing phases approaches zero marks the phase-transition temperature.

DFT calculations have been successfully employed to calculate the free energies of different structural phases and to predict critical temperatures for a wide range of systems, including bulk materials [43], surfaces [44], and quasi-one-dimensional structures [45]. Within this approach, we have previously obtained reasonable results for the Curie temperature of the ferroelectric-paraelectric transition of barium titanate [46].

The temperature-dependent free energies calculated for ferroelectric (black curve) and paraelectric (red curve) LT and LN computed either at the theoretical equilibrium volume $\Omega^{\mathrm{FE}}_{\mathrm{Theory}}$ and $\Omega^{\mathrm{PE}}_{\mathrm{Theory}}$, respectively, or at the common larger volume $\Omega^{\mathrm{PE}}_{\mathrm{Expt}}$ experimentally measured at 940 K, are shown in Fig. 4. In the case of LN, we calculate the free energies based on the results reported in Ref. [7], in which the same PBEsol exchange-correlation functional as used here was employed.

In the case of lithium tantalate the differences of the ground-state energies between the two phases are 0.127 and 0.115 eV for primitive unit cell for $\Omega^{\mathrm{FE/PE}}_{\mathrm{Theory}}$ and $\Omega^{\mathrm{PE}}_{\mathrm{Expt}}$, respectively. The free-energy differences compensate these values in both cases for temperatures above about 800 K, which can thus be considered as a lower bound for the

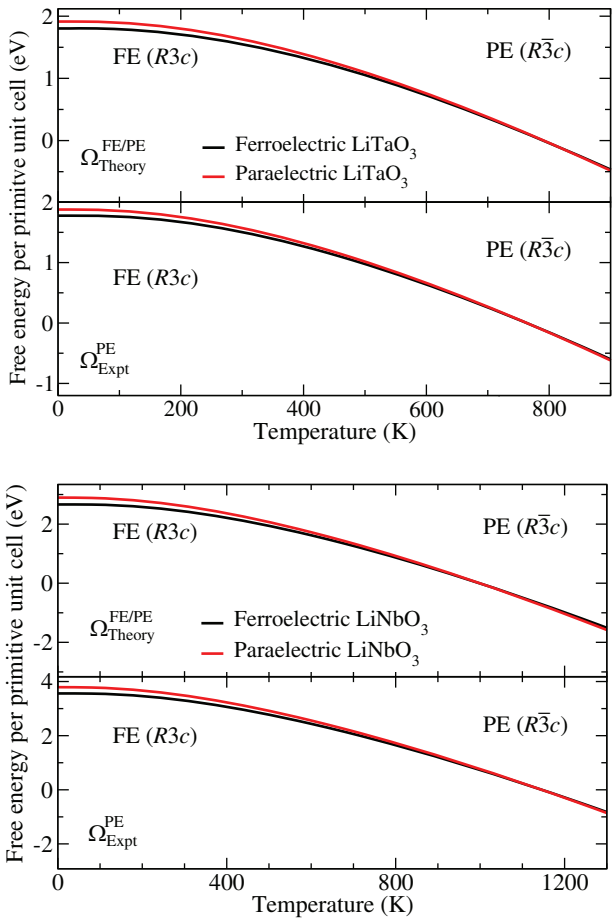

Figure 4 Free energy F of the ferroelectric (black curve) and paraelectric phase (red curve) of $LiTaO_3$ and $LiNbO_3$ calculated at the theoretical (top panel) and at the experimental volume (bottom panel).

transition temperature. The experimental value determined by Bhaumik et al. [35] is 958 K.

For LN, the difference between the electronic ground-state energies of the ferro- and paraelectric phase at the theoretical volumes amounts to 0.259 eV, which is comparable to the difference obtained with similar methods in previous studies [48, 47]. This leads to a lower bound for the transition temperature of about 1000 K, which is about 480 K lower than the measured value. Part of this discrepancy is related to the thermal lattice expansion. In order to take this effect into account, we re-evaluate the electronic ground-state energy and the vibrational frequencies using the larger unit-cell volume measured for temperatures near the phase transition as explained in Section 2. The corresponding results are labeled with Ω^{PE}_{Expt}. The difference between the electronic ground-state energies than increases to 0.262 eV. Using the corresponding phonon frequencies at Ω^{PE}_{Expt} to estimate the free energies, raises the predicted lower bound for the transition temperature by about 160 K.

The better agreement with the experimental value for LT than for LN is at least partially due to the lower value of the Curie temperature. At temperatures around 800 K the lattice vibrations are less affected by anharmonicities than in the case of LN at temperatures around 1200 K, which clearly reduces the uncertainty of our calculations.

Even if both the absolute values as well as the differences between the estimated lower bounds for the Curie temperatures of $LiNbO_3$ and $LiTaO_3$ are in qualitative agreement with the measured values, a word of caution is in order regarding the interpretation of our results. Indeed, two major approximations enter in our approach. The first concerns the free-energy calculations for the paraelectric phases. Due to the fact that some atoms move in an anharmonic double-well potential, imaginary frequencies occur. These cannot be directly included in Eq. (1). Since a high number of **q** points is needed to reach convergence of the vibrational energy, the typical approaches used to cope with this problem for single frequencies [42] are not feasible here. Therefore, we treat all frequencies, including the imaginary frequencies, as being harmonic, i.e., we consider the absolute value. The second approximation is the harmonic approximation itself. The present calculations neglect higher-order effects, such as phonon-phonon coupling, which become relevant at the high temperatures at which the phase transitions of LT and LN occur.

Thus, the predicted values should be considered as rough estimates of the lower bounds of the transition temperatures. We remark that first-principles molecular dynamics [17, 6] indicates that the ferroelectric transition is a second-order structural transition that has mainly order–disorder character.

4 Conclusions We have computed the phonon dispersion and density of states of lithium tantalate from first principles within DFPT. The calculated lattice parameters and phonon frequencies at the Γ point are in very good agreement with available experimental data. Furthermore, we provide the first theoretical modeling of the LO frequencies within DFPT. On the basis of our calculations, we confirm the assignment of the LO phonons proposed in recent spectroscopic experiments [4]. The phonon density of states was used to compute the specific heat capacity of the investigated material. The calculated value of 402 $J\,kg^{-1}\,K^{-1}$ for $LiTaO_3$ is in very good agreement with experimental measurements [41]. The phonon dispersion was further employed to calculate the temperature-dependent free energies of the ferroelectric and paraelectric phases of $LiTaO_3$ and $LiNbO_3$. The presence of phonons with imaginary frequencies in most of the reciprocal space in the paraelectric phase as found in recent molecular-dynamics simulations [6] is compatible with an order–disorder transition type.

Acknowledgements All the calculations were performed at the Paderborn Center for Parallel Computing (PC^2). We gratefully acknowledge financial support by the Deutsche Forschungsgemeinschaft (DFG) via Sonderforschungsbereich TRR 142.

References

[1] R. S. Weis and T. K. Gaylord, Appl. Phys. A **37**, 191 (1985).

[2] A. Räuber, Chemistry and Physics of Lithium Niobate, Current Topics in Materials Science (North-Holland, Amsterdam, 1978).
[3] K. Uchino, Ferroelectric Devices, 2nd edn. (CRC Press, Boca Raton, 2009).
[4] S. Margueron, A. Bartasyte, A. M. Glazer, E. Simon, J. Hlinka, I. Gregora, and J. Gleize, J. Appl. Phys. **111**, 104105 (2012).
[5] S. Sanna, S. Neufeld, M. Rüsing, G. Berth, A. Zrenner, and W. G. Schmidt, Phys. Rev. B **91**, 224302 (2015).
[6] K. Toyoura, M. Ohta, A. Nakamura, and K. Matsunaga, J. Appl. Phys. **118**, 064103 (2015).
[7] M. Friedrich, A. Riefer, S. Sanna, W. G. Schmidt, and A. Schindlmayr, J. Phys.: Condens. Matter **27**, 385402 (2015).
[8] A. S. Barker and R. Loudon, Phys. Rev. **158**, 433 (1967).
[9] W. D. Johnston, Jr. and R. Loudon, Phys. Rev. **168**, 1045 (1968).
[10] J. L. Servoin and F. Gervais, Solid State Commun. **31**, 387 (1979).
[11] M. R. Chowdhury, G. E. Peckham, and D. H. Saunderson, J. Phys. C **11**, 1671 (1978).
[12] Y. Okamoto, P. C. Wang, and J. F. Scott, Phys. Rev. B **32**, 6787 (1985).
[13] S. Kojima, Ferroelectrics **223**, 63 (1999).
[14] H. Lehnert, H. Boysen, F. Frey, A. Hewat, and P. Radaelli, Z. Kristallogr. **212**, 712 (1997).
[15] S. R. Phillpot and V. Gopalan, Appl. Phys. Lett. **84**, 1916 (2004).
[16] D. Lee, H. Xu, V. Dierolf, V. Gopalan, and S. R. Phillpot, Phys. Rev. B **82**, 014104 (2010).
[17] S. Sanna and W. G. Schmidt, IEEE Trans. Ultrason. Ferroelectr. Freq. Control **59**, 1925 (2012).
[18] E. J. Samuelson and A. P. Grande, Z. Phys. B **24**, 207 (1976).
[19] J. L. Servoin and F. Gervais, Ferroelectrics **21**, 563 (1978).
[20] P. Hohenberg and W. Kohn, Phys. Rev. **136**, B864 (1964).
[21] W. Kohn and L. J. Sham, Phys. Rev. **140**, A1133 (1965).
[22] N. E. Zein, Fiz. Tverd. Tela (Leningrad) **26**, 3024 (1984) [Sov. Phys. Solid State **26**, 1825 (1984)].
[23] X. Gonze, Phys. Rev. B **55**, 10337 (1997).
[24] X. Gonze and C. Lee, Phys. Rev. B **55**, 10355 (1997).
[25] S. Baroni, P. Giannozzi, and A. Testa, Phys. Rev. Lett. **58**, 1861 (1987).
[26] X. Gonze, Z. Kristallogr. **220**, 558 (2005).
[27] X. Gonze, B. Amadon, P.-M. Anglade, J.-M. Beuken, F. Bottin, P. Boulanger, F. Bruneval, D. Caliste, R. Caracas, M. Cote, T. Deutsch, L. Genovese, Ph. Ghosez, M. Giantomassi, S. Goedecker, D. R. Hamann, P. Hermet, F. Jollet, G. Jomard, S. Leroux, M. Mancini, S. Mazevet, M. J. T. Oliveira, G. Onida, Y. Pouillon, T. Rangel, G.-M. Rignanese, D. Sangalli, R. Shaltaf, M. Torrent, M.J. Verstraete, G. Zerah, and J. W. Zwanziger, Comput. Phys. Commun. **180**, 2582 (2009).
[28] M. A. L. Marques, M. J. T. Oliveira, and T. Burnus, Comput. Phys. Commun. **183**, 2227 (2012).
[29] J. P. Perdew, A. Ruzsinszky, G. I. Csonka, O. A. Vydrov, G. E. Scuseria, L. A. Constantin, X. Zhou, and K. Burke, Phys. Rev. Lett. **100**, 136406 (2008).
[30] D. R. Hamann, Phys. Rev. B **88**, 085117 (2013).
[31] H. J. Monkhorst and J. D. Pack, Phys. Rev. B **13**, 5188 (1976).
[32] H. B. Schlegel, J. Comput. Chem. **3**, 214 (1982).
[33] C. Thierfelder, S. Sanna, A. Schindlmayr, and W. G. Schmidt, Phys. Status Solidi C **7**, 362 (2010).
[34] A. Riefer, S. Sanna, and W. G. Schmidt, Ferroelectrics **447**, 78 (2013).
[35] I. Bhaumik, S. Ganesamoorthy, R. Bhatt, A. K. Karnal, V. K. Wadhawan, P. K. Gupta, K. Kitamura, S. Takekawa, and M. Nakamura, J. Appl. Phys. **103**, 014108 (2008).
[36] S. C. Abrahams, E. Buehler, W. C. Hamilton, and S. J. Laplaca, J. Phys. Chem. Solids **34**, 521 (1973).
[37] S. C. Abrahams, H. J. Levinstein, and J. M. Reddy, J. Phys. Chem. Solids **27**, 1019 (1966).
[38] L. He, F. Liu, G. Hautier, M. J. T. Oliveira, M. A. L. Marques, F. D. Vila, J. J. Rehr, G.-M. Rignanese, and A. Zhou, Phys. Rev. B **89**, 064305 (2014).
[39] P. Hermet, M. Veithen, and P. Ghosez, J. Phys.: Condens. Matter **19**, 456202 (2007).
[40] K. Parlinski, Z. Q. Li, and Y. Kawazoe, Phys. Rev. B **61**, 272 (2000).
[41] A. M. Glass, Phys. Rev. **172**, 564 (1968).
[42] N. D. Drummond and G. J. Ackland, Phys. Rev. B **65**, 184104 (2002).
[43] F. Körmann, A. Dick, B. Grabowski, B. Hallstedt, T. Hickel, and J. Neugebauer, Phys. Rev. B **78** 033102 (2008).
[44] M. Valtiner, M. Todorova, G. Grundmeier, and J. Neugebauer, Phys. Rev. Lett. **103**, 065502 (2009).
[45] S. Wippermann and W. G. Schmidt, Phys. Rev. Lett. **105**, 126102 (2010).
[46] S. Sanna, C. Thierfelder, S. Wippermann, T. P. Sinha, and W. G. Schmidt, Phys. Rev. B **83**, 054112 (2011).
[47] W. G. Schmidt, M. Albrecht, S. Wippermann, S. Blankenburg, E. Rauls, F. Fuchs, C. Rödl, J. Furthmüller, and A. Hermann, Phys. Rev. B **77**, 035106 (2008).
[48] I. Inbar and R. E. Cohen, Phys. Rev. B **53**, 1193 (1996).